Near-inertial waves extract energy from barotropic turbulence: freely-evolving flow

Cesar B. Rocha[1]†, Gregory L. Wagner[2] and William R. Young[1]

[1]Scripps Institution of Oceanography, University of California, San Diego

[2]Department of Earth, Atmospheric and Planetary Sciences, Massachusetts Institute of Technology

(Received xx; revised xx; accepted xx)

Key words:

1. Introduction

The closing of the ocean's energy budget remains poorly understood, largely because geostrophic turbulence transfers energy towards large scales. Existing studies suggest a panoply of ageostrophic mechanisms to account for the required forward flow of energy. These include (but are not limited to) surface and benthic boundary turbulence and wave generation by geostrophic eddies sloshing over bottom topography (see Nagai *et al.* 2015, their figure 1, and references therein). But roughly half of the energy flux out of the ocean mesoscales remains unaccounted for.

Recent studies suggest that the interaction of geostrophic flows with externally-forced (windy) internal waves serves as a major sink of mesoscale energy en route to viscous dissipation (Xie & Vanneste 2015; Taylor & Straub 2016; Wagner & Young 2016; Barkan *et al.* 2016). The emphasis on interactions of geostrophic flow with windy internal waves — here denoted stimulated imbalance† — contrasts with energy loss via spontaneous emission — a process by which internal waves are emitted during geostrophic adjustment (e.g., Shakespeare & Hogg 2017). While spontaneous emission is localized at sharp fronts (large Rossby number, $\mathrm{Ro} \gtrsim 1$) in the surface boundary layer (e.g., Shakespeare & Hogg 2017), stimulated imbalance operates at the small Rossby-number ($\mathrm{Ro} \ll 1$), quasi-geostrophic regime, both in the upper ocean and in the interior (e.g., Xie & Vanneste 2015).

With the goal of understanding the physical mechanisms of energy extraction from barotropic flow by existing internal waves, we here analyze a simple model that contains stimulated imbalance. This minimal model is a special family of solutions of the Xie & Vanneste (2015) equations, which couple the evolution of near-inertial waves (NIWs) with quasigeostrophic (QG) flow. The focus on QG-NIW interactions is justified: geostrophic eddies account for the bulk of the ocean's eddy kinetic energy (90%, Ferrari & Wunsch

† Email address for correspondence: crocha@ucsd.edu

† Following Xie & Vanneste (2015) and Wagner & Young (2016) we define *stimulated imbalance* as wave-mean interactions that transfer energy from geostrophic motions (the 'mean flow') to existing internal waves. This definition contrasts with the nomenclature recently employed by Barkan *et al.* (2016), who term stimulated imbalance a process by which internal waves trigger a forward cascade from mesoscale to submesoscale (but subinertial) flows.

2009) and near-inertial waves contain most of the oceanic high-frequency variability (Alford *et al.* 2016). The minimal QG-NIW coupled model transparently reveals the physics of stimulated imbalance associated with vertical vorticity and lateral strain.

2. The physics of NIW energy extraction from a barotropic QG flow

2.1. *The Xie & Vanneste (2015) minimal QG-NIW model*

With barotropic quasigeostrophic flow, $\psi = \psi(x, y, t)$, uniform background buoyancy frequency N_0, and single-mode NIW vertical structure, $\mathrm{e}^{\mathrm{i}mz}$, the Xie & Vanneste (2015) QG-NIW coupled model (Appendix A) reduces to

{macroturb} $$q_t + \mathsf{J}(\psi, q) = 0\,, \tag{2.1}$$

with the NIW-averaged quasigeostrophic potential vorticity (QGPV)

{qgpv} $$q = \triangle\psi + \tfrac{1}{f_0}\left[\tfrac{1}{4}\triangle|\phi|^2 + \tfrac{\mathrm{i}}{2}\mathsf{J}(\phi^\star, \phi)\right], \tag{2.2}$$

and the streamfunction is defined so that the geostrophic flow velocity is $(u_e, v_e) = (-\psi_y, \psi_x)$; and

{waves} $$\phi_t + \mathsf{J}(\psi, \phi) + \tfrac{\mathrm{i}}{2}\phi\triangle\psi - \tfrac{\mathrm{i}}{2}f_0\lambda^2\triangle\phi = 0\,, \tag{2.3}$$

with NIW velocity

w_velocity} $$u_w + \mathrm{i}v_w = \mathrm{e}^{\mathrm{i}(mz - f_0 t)}\phi(x, y, t)\,. \tag{2.4}$$

Above, ϕ is the back-rotated NIW velocity, $\triangle \overset{\text{def}}{=} \partial_x^2 + \partial_y^2$ is the horizontal laplacian, $\mathsf{J}(f, g) = f_x g_y - f_y g_x$ is the horizontal Jacobian, $\lambda = \frac{N_0}{f_0\, m}$ is an intrinsic horizontal scale and the superscript star * denotes complex conjugation.

Similarly to the Young & Ben Jelloul (1997) model, the NIW amplitude ϕ evolves through wave dispersion — the last term in (2.3) — and advection and refraction by the QG flow — the second and third terms in (2.3). But the wave equation (2.3) is non-linear owing to the quadratic wave terms in the *inversion* relation (2.2). In other words, the Young & Ben Jelloul (1997) NIW model is purely kinematic: the QG flow evolves as if there were no waves and set an inhomogeneous medium in which NIWs propagate. But the Xie & Vanneste (2015) model is dynamic because both q and ϕ determine the flow: $\psi = \psi(x, y, t; q, \phi)$. Besides advection and refraction by the QG flow, these QG-NIW interactions imply a positive finite-amplitude frequency shift (Appendix A).

The wave equation (2.3) is similar to the reduced-gravity Young & Ben Jelloul model derived by Danioux *et al.* (2015). Without advection, (2.3) is analogous to Schrodinger's equation (e.g., Landau & Lifshitz 2013, pg. 51), with the vorticity, $\triangle\psi$, playing the role of the potential and the dispersivity, $f_0\lambda^2$, mimicking Planck's constant (Danioux *et al.* 2015).

2.2. *Quadratic invariants and energy conversion*

From (2.3), the near-inertial kinetic energy density $\frac{1}{2}|\phi|^2$ satisfies

on_density} $$\partial_t \tfrac{1}{2}|\phi|^2 + \mathsf{J}(\psi, \tfrac{1}{2}|\phi|^2) + \boldsymbol{\nabla}\cdot\underbrace{\left[\tfrac{\mathrm{i}}{4}f_0\lambda^2\left(\phi\boldsymbol{\nabla}\phi^\star - \phi^\star\boldsymbol{\nabla}\phi\right)\right]}_{\overset{\text{def}}{=}\mathbf{F}_w} = 0\,. \tag{2.5}$$

Locally, $\frac{1}{2}|\phi|^2$ changes due to divergences of the geostrophic and wave fluxes of $\frac{1}{2}|\phi|^2$ — the second and third terms in (2.5). The wave flux $\mathbf{F}_w$ is analogous to the probability current density of quantum mechanics (e.g., Landau & Lifshitz, pg 57). Using the polar

representation $\phi = |\phi| e^{i\Theta}$ (e.g., Klein *et al.* 2004), we can compactly express the wave flux

{Fw2}
$$\mathbf{F}_w = \tfrac{i}{4} f_0 \lambda^2 \left(\phi \boldsymbol{\nabla} \phi^\star - \phi^\star \boldsymbol{\nabla} \phi\right) = f_0 \lambda^2 \boldsymbol{\nabla}\Theta \times \tfrac{1}{2}|\phi|^2 \,. \tag{2.6}$$

The expression on the right of (2.6) makes it explicit that $\mathbf{F}_w$ is a wave flux of kinetic energy density $\frac{1}{2}|\phi|^2$, where $f_0\lambda^2\boldsymbol{\nabla}\Theta = \frac{N_0^2}{f_0 m^2}\boldsymbol{\nabla}\Theta$ is the generalized group velocity of hydrostatic NIWs, which can be quickly verified under the plane-wave assumption $\Theta = kx + ly$.

With simple boundary conditions, e.g., periodic or no normal flux, the QG-NIW model (2.1)-(2.3) conserves NIW kinetic energy

{action}
$$\frac{\mathrm{d}}{\mathrm{d}t} \underbrace{\tfrac{1}{2}\langle |\phi|^2 \rangle}_{\overset{\text{def}}{=} K_w} , \tag{2.7}$$

where angle brackets, $\langle\ \rangle$, represent average over the domain of area $\mathcal{A}$:

{average}
$$\langle\, f \rangle \overset{\text{def}}{=} \frac{1}{\mathcal{A}} \iint_{\mathcal{A}} f \,\mathrm{d}x\mathrm{d}y \,. \tag{2.8}$$

Also from (2.3), we form an equation for the wave potential energy: $\frac{\lambda^4}{4}\langle \triangle\phi^\star \times (2.3) + \triangle\phi \times (2.3)^\star \rangle$ yields

{Pw}
$$\frac{\mathrm{d}}{\mathrm{d}t} \underbrace{\langle \tfrac{\lambda^2}{4} |\boldsymbol{\nabla}\phi|^2 \rangle}_{\overset{\text{def}}{=} P_w} = \underbrace{\tfrac{1}{f_0}\left\langle \tfrac{1}{2}\triangle\psi \boldsymbol{\nabla}\cdot\mathbf{F}_w \right\rangle}_{\overset{\text{def}}{=} \Gamma_r} + \underbrace{\tfrac{\lambda^2}{2}\left\langle \tfrac{1}{2}\left[\triangle\phi^\star \mathsf{J}(\psi,\phi) + \triangle\phi \mathsf{J}(\psi,\phi^\star)\right] \right\rangle}_{\overset{\text{def}}{=} \Gamma_a} . \tag{2.9}$$

Finally, we form an equation for the QG kinetic energy, K_e: $\langle \psi \times (2.1) \rangle$, with (2.2), (2.5), (2.3), and multipliple integration by parts, give

{Ke}
$$\frac{\mathrm{d}}{\mathrm{d}t} \underbrace{\langle \tfrac{1}{2}|\boldsymbol{\nabla}\psi|^2 \rangle}_{\overset{\text{def}}{=} K_e} = -(\Gamma_r + \Gamma_a) \,, \tag{2.10}$$

thus proving that the QG-NIW model (2.1)-(2.3) conserves the coupled energy

{E}
$$E \overset{\text{def}}{=} K_e + P_w \,. \tag{2.11}$$

In (2.10), $\Gamma_r + \Gamma_a$ is the energy conversion between QG kinetic energy and wave potential energy. The term Γ_r stems from refraction and is easy to interpret: the convergence, $\nabla\cdot\mathbf{F}_w < 0$, of the wave flux of NIW kinetic energy density into anticyclones, $\triangle\psi < 0$, is a source of NIW potential energy, P_w.

The term Γ_a stems from advection and is similar to the source of variance of a trace gradient subject to lateral stirring,

{c_t}
$$c_t + \mathsf{J}(\psi, c) = 0. \tag{2.12}$$

From (2.12), we deduce that $\langle \triangle c \mathsf{J}(\psi, c) \rangle$ is the variance production of passive scalar gradient, $\langle |\boldsymbol{\nabla} c|^2 \rangle$. Analogously, Γ_a is the source of wave potential energy due to geostrophic stirring. After multiple integration by parts, we rewrite this term as

{gradphi}
$$\Gamma_a = \left\langle \begin{bmatrix} \phi_x^\star & \phi_y^\star \end{bmatrix} \mathbf{S} \begin{bmatrix} \phi_x \\ \phi_y \end{bmatrix} \right\rangle , \tag{2.13}$$

where $\mathbf{S}$ is the symmetric part of the geostrophic velocity gradient matrix,

$$\mathbf{S} \overset{\text{def}}{=} \begin{bmatrix} -\psi_{xy} & \frac{1}{2}(\psi_{xx}-\psi_{yy}) \\ \frac{1}{2}(\psi_{xx}-\psi_{yy}) & \psi_{xy} \end{bmatrix} , \tag{2.14}$$

whose sum of the elements squared (the Frobenius norm) is commonly defined as the square of the QG rate of strain. Hence, geostrophic straining enhances existing gradients of ϕ, thereby generating wave potential energy, P_w. When the QG flow has a lateral scale much larger than the NIW field, this distortion of ϕ is akin to the wave-capture mechanism of Bühler & McItyre (2005).

2.3. *Averaged equations and loss of coherence*

The domain-averaged potential vorticity $\langle q \rangle$ is invariant as a consequence of the material invariance of q — or the invariance of the average of each individual term in (2.2). The spatially-averaged (coherent) NIW amplitude satisfies

{phi_ave}
$$\frac{\mathrm{d}}{\mathrm{d}t}\langle\phi\rangle + \mathrm{i}\left\langle \tfrac{1}{2}\phi\triangle\psi \right\rangle = 0\,. \tag{2.15}$$

Introducing the decomposition $\phi = \langle\phi\rangle + \phi'$, we have

$$\tfrac{1}{2}\langle|\phi|^2\rangle = \underbrace{\tfrac{1}{2}|\langle\phi\rangle|^2}_{\overset{\text{def}}{=} K^c_w} + \underbrace{\tfrac{1}{2}\langle|\phi'|^2\rangle}_{\overset{\text{def}}{=} K^i_w}, \tag{2.16}$$

Thus, the kinetic energy of horizontally incoherent (ϕ') and coherent ($\langle\phi\rangle$) NIW amplitude satisfy

{Kiw}
$$\dot{K}^i_w = \Pi\,, \tag{2.17}$$

and

{Kcw}
$$\dot{K}^c_w = -\Pi\,, \tag{2.18}$$

with the kinetic energy transfer

{Pi}
$$\Pi = \tfrac{\mathrm{i}}{2}\left[\langle\tfrac{1}{2}\phi\triangle\psi\rangle\langle\phi^\star\rangle - \langle\tfrac{1}{2}\phi^\star\triangle\psi\rangle\langle\phi\rangle\right]\,. \tag{2.19}$$

The decay of a laterally coherent near-inertial oscillation due to refraction by geostrophic flow is relevant for mixed-layer slab models used to estimate the work imparted by wind into the NIW field (e.g., Alford 2001). Without further assumptions, it is unclear if the effect of refraction is sign definite. If the NIWs have initial larger scales than the geostrophic field, then refraction generates eddy-scale perturbations, implying a reduction of lateral coherence ($\Pi > 0$). But it remains unclear if this transfer can be parameterized as a linear damping.

2.4. *Relevant parameters*

Using the scaling

$$\psi \sim U_e k_e^{-1}\,, \qquad \text{and} \qquad \phi \sim U_w\,, \tag{2.20}$$

with characteristic QG and NIW velocity scales U_e and U_w, and the characteristic horizontal length scale k_e^{-1} and time scale $(U_e k_e)^{-1}$, reveals that there are two dynamically relevant parameters of the QG-NIW problem described by (2.1)-(2.3). First, the 'wave amplitude'

{alpha}
$$\alpha \overset{\text{def}}{=} \underbrace{\frac{U_e k_e}{f_0}}_{\overset{\text{def}}{=} Ro} \times \left(\frac{U_w}{U_e}\right)^2, \tag{2.21}$$

measures the strength of the waves compared to the geostrophic flow and scales the contribution of the NIW terms to the QGPV. Second, the 'wave dispersivity,'

{hslash}
$$\hbar \stackrel{\text{def}}{=} f_0 \lambda^2 \times \frac{k_e}{U_e}\,, \tag{2.22}$$

scales the importance of linear dispersion, which counteracts the unsmoothing effects of advection and refraction.

Also, the two conversion terms, Γ_r and Γ_a, scale with the same non-dimensional parameter $\alpha \times \hbar$. But this does not imply that the energy conversion scales linearly with both wave amplitude and dispersivity: the scales developed by the NIW amplitude field ϕ and the correlations in Γ depend on α and $\hbar$

2.5. *Summary*

We can summarize the physics of stimulated imbalance considering an initial value problem that idealizes the oceanographic 'post-storm' context: stormy winds impart momentum into the ocean, thereby generating near-inertial oscillations with a lateral decorrelation scale larger than the mesoscale eddies. The after-storm evolution of an initially large-scale coherent inertial oscillation is described by (2.1)–(2.3) (Xie & Vanneste 2015). Geostrophic refraction focus NIWs in anticyclones. The eddy-scale gradients of ϕ then support geostrophic advection. Advection and refraction reduce the lateral coherence of NIWs — and wave dispersion counteracts this unsmoothing effect.

The explicit expression for energy conversion on the right of (2.9) enlightens the physics of the problem. Refraction causes a convergence of NIW kinetic energy density in anticyclones. And advection strains the NIW field, enhancing gradients of ϕ. Both processes generate NIW potential energy at the expenses of geostrophic kinetic energy, thus motivating the nomenclature 'refraction sink' ($-\Gamma_r$) and 'advection sink' ($-\Gamma_a$) of QG kinetic energy.

The remaining of this paper verifies this thought experiment by solving numerically two problems in which an initially perfectly coherent near-inertial oscillation interacts with the Lamb dipole (Section 3) and with a turbulent field emergent from random initial conditions (Section 4).

3. The Lamb-Chaplygin dipole

The Lamb-Chaplygin dipole is an exact solution of the Euler equations on an infinite two-dimensional plane where the vorticity is confined to a circle of radius R (Meleshko & Van Heijst 1994). The solution, steady on a frame moving at uniform zonal velocity U, is

{lambd_q}
$$\triangle\psi = \frac{2U\kappa}{J_0(\kappa R)} \begin{cases} J_1(\kappa r)\sin\theta\,, & \text{if} \quad r \leqslant R\,, \\ 0\,, & \text{if} \quad r \geqslant R\,, \end{cases} \tag{3.1}$$

where $r^2 = (x - x_c)^2 + (y - y_c)^2$ is the radial distance about the dipole's center (x_c, y_c), $\tan\theta = (y - y_c)/(x - x_c)$, and J_n is the n'th order Bessel function of first kind. The matching condition at $r = R$, $J_1(\kappa R) = 0$, determines κ. The dipole is the first eigensolution, with eigenvalue $\kappa R \approx 3.8287$. If the wave QGPV is zero, then the dipole (3.1) is a solution of (2.1). This is the case when a uniform ϕ is used as initial condition (Sections 3 and 4).

While we perform the calculations with dimensional variables, we non-dimensionalize the results for clarity. For the dipole (3.1), we use $U_e = U$ and $k_e = 2\pi/R$. As for

the initial NIW amplitude, we consider a uniform (i.e., perfectly coherent) near-inertial oscillation with speed U_w:

$$\phi(x, y, t = 0) = \tfrac{1+\mathrm{i}}{\sqrt{2}}\, U_w\,. \tag{3.2}$$ {NIO}

3.1. *Parameter inspired by the Ocean Storms Experiment*

The Lamb-Chaplygin dipole provides a compact and weak vortex flow. Inspired by the Ocean Storms Experiments (D'Asaro *et al.* 1995), we choose $U_e = 5 \times 10^{-2}$ m s^{-1}, $R = 2\pi/k_e = 84$ km, and $f_0 = 10^{-4}$ s^{-1} (~ 45°N), which gives Ro $\approx 3.75 \times 10^{-2}$. Strong storm over weak mesoscale flow generates strong near-inertial currents (D'Asaro *et al.* 1995). Choosing $U_w = 10 \times U_e = 10^{-1}$m s^{-1} yields a wave amplitude $\alpha \approx 3.75$. A NIW with a typical vertical wavelength, $2\pi/m = 325$ m, on a moderately-stratified upper-ocean, $N = 50 \times f_0 = 5 \times 10^{-3}$ s^{-1}, yields a moderate dispersivity $\hbar \approx 1$.

3.2. *Solution for $\hbar \approx 1$ and $\alpha \approx 3.75$*

We solve the QG-NIW system (2.1)-(2.3) subject to the initial conditions (3.1) and (3.2) and the parameters inspired by the Ocean Storms Experiment. We integrate the solutions numerically for 30 eddy-turnover time units, $30 \times (U_e k_e)^{-1} \approx 90$ days, on a doubly periodic domain using standard Fourier pseudo-spectral methods (Appendix B). Dipole images, an artifact of periodization, cause a small zonal drift of the dipole. To render this effects negligible, we choose a domain size much larger than the dipole's radius, $R/L \approx 0.06$. Table B.1 provides a full description of solution parameters.

Because the initial NIW wave amplitude is laterally uniform, refraction dominates the initial evolution of the solution. Indeed, the solution presents a dramatic wave concentration in the anticyclone and wave expulsion from the cyclone in the first couple of eddy turnover time units, $(U_e k_e)^{-1}$. After $5 \times (U_e k_e)^{-1}$, there is a threefold modulation of the wave kinetic energy density on eddy scales (Figure 3.2). The correlation coefficient

$$r \overset{\text{def}}{=} \frac{\left\langle |\phi'|^2 \triangle\psi \right\rangle}{\left\langle |\phi'|^4 \right\rangle^{1/2} \left\langle (\triangle\psi)^2 \right\rangle^{1/2}}\,, \tag{3.3}$$ {corr_r}

quantifies the wave concentration in regions positive or negative vorticity. Negative correlation, $r < 0$, indicates wave concentration in anticyclones (Danioux *et al.* 2015). Starting form the uniform wave initial condition, vorticity and incoherent wave kinetic energy density quickly becomes negatively correlation ($r = -0.75$ at $t \times U_e k_e = 2$; Figure 3.2d). This initial wave focusing in anticyclones is associated with a rapid increase in incoherent wave kinetic energy (Figure 3.2c) and generation of wave potential energy (Figure 3.2b). The gain of wave potential energy, ininitially dominated by the conversion due to refraction , Γ_r, occurs at the expenses of quasigeostrophic kinetic energy (Figure 3.2a): the dipole's kinetic energy decays by about 20% in two eddy-turnover time units. The strong wave concentration in the negative vorticity region, and the accompanying energy loss, weakens the anticyclone. This asymmetry tilts the dipole and the self-induced velocity no longer matches the zonal upstream uniform flow: the dipole starts to drift downstream at $t \times U_e k_e \approx 5$.

The eddy-scale gradients in wave amplitude, which are created by refraction, allow for the other mechanisms in the wave equation (2.3) to become important. Linear dispersion radiates waves, with horizontal scales comparable to k_e^{-1}, from the dipole. And geostrophic advection starts to enhance the refraction-created gradients. As a consequence of these two processes becoming important, the correlation r decreases.

The advective conversion, Γ_a, kicks off at $t \times U_e k_e \approx 4$ (Figure 3.2b), and takes over the Γ in few eddy-turnover time units. Contemporarily, the wave-induced quasigeostrophic

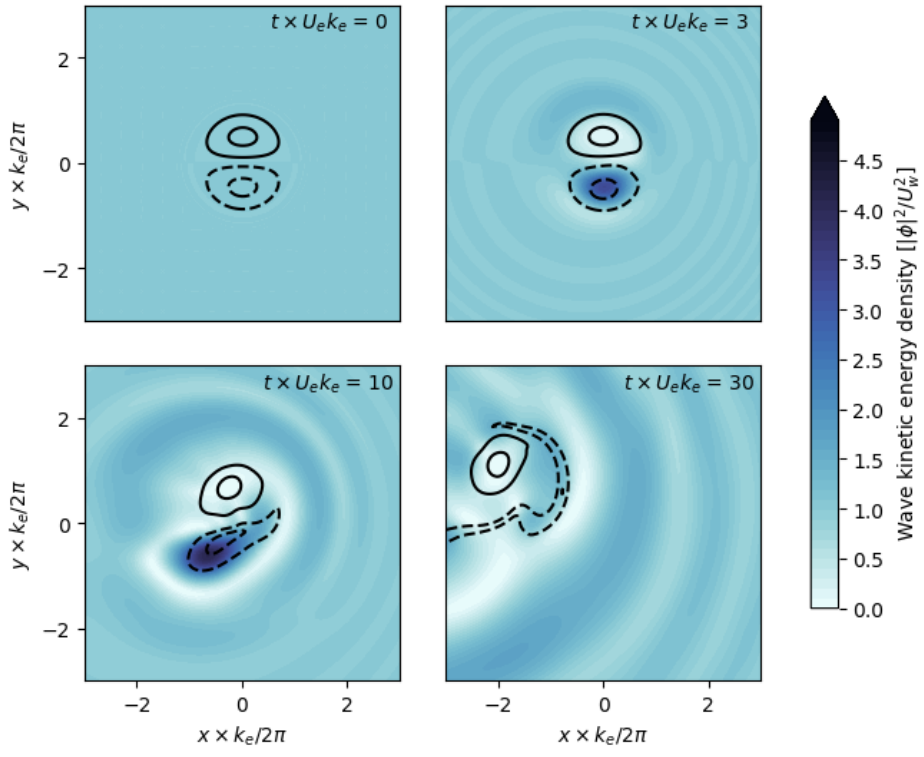

FIGURE 1. Snapshots of the Lamb-Chaplygin dipole solution with $\hbar \approx 1$ and $\alpha \approx 3.75$. Colors represent wave kinetic energy density, $|\phi'|^2/U_w^2$. Contours represent potential vorticity, $q/(U_e k_e) = [-1.5, -0.5, 1.5, 0.5]$, with dashed lines showing negative values. These plots only show the central $(1/5)^2$ of the simulation domain. (The supplemental material contains a video of the simulation.)

flow strains the anticyclone, which develops a filamentary structure. Because most of the advective energy conversion occurs in the anticyclone, the correlation r decreases further, becoming positive at $t \times U_e k_e \approx 7$, and Γ_r becomes weakly negative.

4. Decaying Macroturbulence

To study the QG-NIW interaction and energy exchange in a turbulent regime relevant to the ocean, we consider a barotropic turbulence flow that emerges from random initial conditions integrated for 20 eddy turnover time units. In other words, we first integrate the initial condition

$$\psi\big(x, y, t \times U_e k_e = -20\big) = \sum_{k,l} |\hat{\psi}| \cos\left(kx + ly + \chi_{k,l}\right) \tag{4.1}$$ {psi_init

with waveless QG dynamics before introducing waves at $t \times U_e k_e = 0$. In 4.1, $\chi_{k,l}$ is a random phase uniformly distributed on $[0, 2\pi)$, and $|\hat{\psi}|$ is the isotropic spectrum

$$|\hat{\psi}| = C \times \left\{|k|\left[1 + (|k|/k_e)^4\right]\right\}^{-1/2}, \tag{4.2}$$ {psih_mag

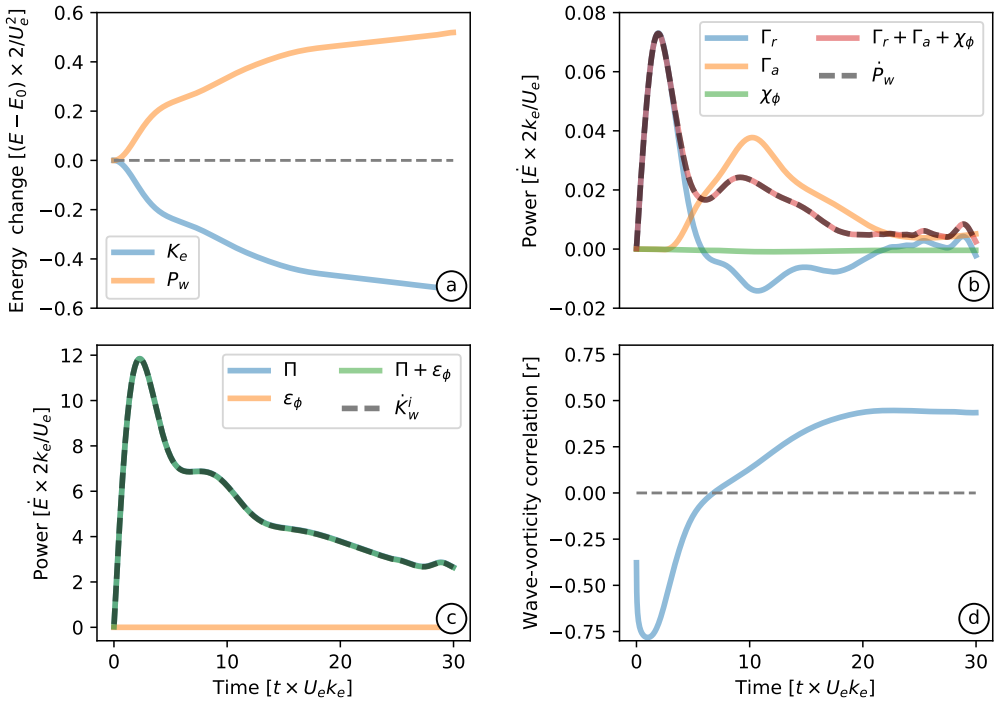

FIGURE 2. Statistics of the Lamb-Chaplygin dipole solution with $\hbar \approx 1$ and $\alpha \approx 3.75$. (a) Energy change about initial condition. (b) Wave potential energy budget (2.9). (c) Incoherent wave kinetic energy budget (2.17). (d) Coefficient of correlation between incoherent wave kinetic energy and relative vorticity (3.3).

with the wavenumber magnitude $|k|^2 = k^2 + l^2$. The prescribed initial energy $U_e^2/2$ determines the constant C:

$$\sum_{k,l} \underbrace{|k|^2|\hat{\psi}|^2}_{\stackrel{\text{def}}{=}\mathcal{K}_e} = \tfrac{1}{2}U_e^2\,. \tag{4.3}$$ {ke_init}

The kinetic energy spectrum $\mathcal{K}_e$ peaks at the energy-containing scale k_e^{-1}. At scales smaller than k_e^{-1}, $\mathcal{K}_e$ has a linear dependence on $|k|$, whereas it decays as $|k|^{-3}$ at scales larger than k_e^{-1}. This red spectrum ensures insignificant energy dissipation by the biharmonic viscosity added to (2.1) to absorb the forward cascade of enstrophy (Appendix B).

The evolution of a random initial condition constrained by the inviscid dynamics (2.1) has been well studied, beginning with Fornberg (1977). Stirring of vorticity $\triangle\psi$ by the flow ψ transfers enstrophy towards small scales; energy flows to large scales. Most of enstrophy dissipated within few eddy turnover time units, whereas kinetic energy is nearly conserved. Vorticity concentrates into localized structures: after 20 eddy turnover time units, the vorticity is well-organized into a sea of coherent vortices that form via like-sign vortex merging (e.g., McWilliams 1984).

We add a perfectly coherent near-inertial oscillation (3.2) to the mature barotropic turbulence at $t \times U_e k_e = 0$. For all parameters considered in the remaining of this paper, there are no qualitative long-term differences between the solutions described below and results from introducing the waves at $t \times U_e k_e = -20$.

4.1. *Parameters for strong mid-latitude macroturbulence*

Consider strong mid-latitude macroturbulence, such as the Gulf Stream or Kuroshio Extension. The choice of parameters, $U_e = 0.1$ m s^{-1}, $f_0 = 1\times10^{-4}$ s^{-1}, $2\pi k_e^{-1} = 125$ km gives a Rossby number $Ro \approx 0.05$. For reference, the eddy-turnover scale is $(U_e k_e)^{-1} \approx 5.8$ days. Strong NIW velocity imparted by atmospheric storms, $U_w \sim \sqrt{2}U_e$, implies a wave amplitude

$$\alpha \approx 0.1\,. \tag{4.4}$$

A NIW vertical wavelength of $\lambda_z = 2\pi/m = 300$ m (e.g., Alford *et al.* 2016) on a strongly stratified upper-ocean $N_0/f_0 = 100$ yields a dispersivity

$$\hbar \approx 1.0\,. \tag{4.5}$$

4.2. *Solutions for $\hbar = 1$ and $\alpha = 0.1$*

4.3. *Parameter exploration*

5. Final Remarks

Appendix A. Details of the QG-NIW model

A.1. *The Xie & Vanneste (2015) model*

Xie & Vanneste (2015) derive the QG-NIW model using a variational formulation of the generalized Lagrangian mean (GLM) framework with Whitham averaging. Following Young & Ben Jelloul (1997), Xie & Vanneste write the NIW velocity in complex form

$$u_w + \mathrm{i}v_w = M_z \mathrm{e}^{-\mathrm{i}f_0 t}\,. \tag{A 1}$$

Their derivation recovers the wave equation that governs the evolution of the NIW complex amplitude M_z,

$$M_{zzt} + \partial_z \mathsf{J}(\psi, M_z) + \tfrac{\mathrm{i}}{2}\left[\left(\frac{N^2}{f_0} + \psi_{zz}\right)\triangle M - 2\nabla\psi_z\cdot\nabla M_z + M_{zz}(\triangle\psi + 2\beta y)\right] = 0\,, \tag{A 2}$$

with the QG streamfunction $\psi(x, y, z, t)$. The QG flow evolves through stirring of QGPV

$$q_t + \mathsf{J}(\psi, q) = 0\,. \tag{A 3}$$

A fundamental difference is that the QGPV in the Xie & Vanneste (2015) model contains quadratic wave terms

$$q = \nabla\psi + \left(\tfrac{f_0^2}{N^2}\psi_z\right)_z + \beta y + \tfrac{\mathrm{i}}{2f_0}\mathsf{J}(M_z^\star, M_z) + \tfrac{1}{4f_0}\left(2|\nabla M_z|^2 - M_{zz}^\star\nabla M - M_{zz}\nabla M^\star\right)\,. \tag{A 4}$$

Hence, NIWs actively evolve, affecting the QG flow. The model of Xie & Vanneste (2015), with the potential vorticity that includes wave terms, generalizes early ideas introduced by Bühler & McIntyre (1998) to a setup that avoids spatial scale separation between geostrophic flow and waves, but restricts attention to near-inertial frequencies. Using standard perturbation theory, Wagner & Young (2016) contemporarily recovered and extended this coupled QG-NIW system.

The special family of solutions with barotropic, f-plane QG flow, uniform background stratification, and single vertical mode NIW, $M_z = \phi(x, y)\mathrm{e}^{\mathrm{i}mz}$, yields the reduced set of equations (2.1)-(2.3) used in this paper.

A.2. *Wave self-interaction and frequency shift*

To gain further insight into the dynamics, we decompose the balanced flow into 'vorticity-induced' and 'wave-induced' fields, $\psi = \psi^q + \psi^w$, where

$$\triangle\psi^q = q\,, \qquad \text{and} \qquad \triangle\psi^w = -\frac{1}{4f_0}\triangle|\phi|^2 - \tfrac{\mathrm{i}}{2f_0}\mathsf{J}(\phi^\star,\phi)\,. \tag{A 5}$$ {q_qw}

With the (A 5) decomposition, the QGPV equation (2.1) becomes

$$\triangle\psi^q_t + \mathsf{J}(\psi^q+\psi^w, \triangle\psi^q) = 0\,. \tag{A 6}$$ {lpsiq_t}

In other words, the relative vorticity of the 'vorticity-induced' flow changes due to advection by the total flow $\psi^q + \psi^w$. The wave equation satisfies

$$\underbrace{\left(\partial_t - \tfrac{\mathrm{i}}{2}f_0\lambda^2\triangle\right)\phi}_{\text{Lin. wave dynamics}} + \underbrace{\mathsf{J}(\psi^w,\phi) + \tfrac{\mathrm{i}}{2}\phi\triangle\psi^w}_{\text{Non-lin. wave dynamics}} + \underbrace{\mathsf{J}(\psi^q,\phi) + \tfrac{\mathrm{i}}{2}\phi\triangle\psi^q}_{\text{Adv./refrac. by }\psi^q} = 0\,. \tag{A 7}$$ {waves2}

From (A 5), the 'wave-induced' streamfunction ψ^w is quadratic in ϕ:

$$\psi^w = \tfrac{1}{4f_0}|\phi|^2 + \tfrac{\mathrm{i}}{2f_0}\triangle^{-1}\mathsf{J}(\phi^\star,\phi)\,, \tag{A 8}$$ {psiw}

where $\triangle^{-1}$ is the inverse of the Laplacian: $\triangle^{-1}\triangle f = f$.

Together, equations (A 7)-(A 8) show the non-linear nature of the wave equation in this coupled QG-NIW model. In particular, the non-linear wave dynamics is cubic in wave amplitude. Dropping these cubic wave terms yields a quasi-linear (QL) QG-NIW system. This QL system conserves the energy

$$E_{ql} \overset{\text{def}}{=} \langle \tfrac{1}{2}|\boldsymbol{\nabla}\psi^q|^2\rangle + \langle \boldsymbol{\nabla}\psi^q\cdot\boldsymbol{\nabla}\psi^w\rangle + \langle \tfrac{\lambda^2}{4}|\boldsymbol{\nabla}\phi|^2\rangle\,. \tag{A 9}$$

Note that $\mathrm{E} = E_{ql} + \langle \frac{1}{2}|\boldsymbol{\nabla}\psi^w|^2\rangle$. Thus, the QL approximation is an intermediate model between the uncoupled QG-YBJ model ($\psi^w = 0$) and the non-linear coupled QG-NIW model.

To study the non-linear wave effects, we linearize the QG-NIW equations about the exact solution $\phi = \Phi =$ constant and $\psi = 0$, so that $q = 0$. The QGPV equation (2.1) linearized about this state is trivial: $q_t = \triangle\psi^q_t = 0$, thus $\triangle\psi^q$ remains zero. Also,

$$\triangle\psi^w = -\tfrac{\Phi}{2f_0}\triangle\tfrac{1}{2}(\phi+\phi^\star)\,, \tag{A 10}$$ {lin_q}

where ϕ represents the small departure about the constant Φ, so that the linearized wave equation becomes

$$\phi_t = \tfrac{\mathrm{i}}{2}\left[\tfrac{\Phi^2}{2f_0}\triangle\tfrac{1}{2}(\phi+\phi^\star) + f_0\lambda^2\triangle\phi\right]\,. \tag{A 11}$$

Recalling that $u_w + \mathrm{i}v_w = \phi\mathrm{e}^{\mathrm{i}(mz - f_0 t)}$, we recast the wave equation:

$$\left[\partial_t^2 - \tfrac{1}{4}f_0\lambda^2\left(f_0\lambda^2 + \frac{\Phi^2}{2f_0}\right)\triangle^2\right]v_w = 0\,, \tag{A 12}$$

where $\triangle^2 = (\partial_x^2+\partial_y^2)^2$. Hence, plane-wave solutions yield the dispersion relation

$$\omega = \tfrac{1}{2}f_0\lambda^2(k^2+l^2)\left[1 + \tfrac{1}{2}\tfrac{\Phi^2}{f_0^2\lambda^2}\right]^{1/2}\,, \tag{A 13}$$

and we conclude that the wave self-interaction shifts the frequency by

$$\left[1 + \tfrac{1}{2}\tfrac{\Phi^2}{f_0^2\lambda^2}\right]^{1/2} - 1\,. \tag{A 14}$$

Appendix B. Details of the initial value problems

B.1. *Small-scale dissipation*

To absorb the forward cascade of enstrophy, we add a biharmonic viscosity to the potential vorticity equation (2.1)

$$-\nu_e \triangle^2 q\,, \tag{B 1}$$

where $\triangle^2 = (\partial_x^2 + \partial_y^2)^2$. Similarly, to prevent the development of very small scales, which may violate the near-inertial approximation, we add a biharmonic viscosity in the wave equation (2.3)

$$-\nu_w \triangle^2 \phi\,. \tag{B 2}$$

We find that this choice of small-scale dissipation is sufficient to extend the spectral resolution compared to Laplacian viscosity, while minimizing obscure physical effects associated with higher-order hyperviscosities or spectral filters (McWilliams 1984). In practice, we choose the hyperviscous coefficients that place the 35% highest modes in the dissipation range, so that aliased wavenumbers are strongly damped.

These hyperviscous terms add small dissipation to the energy equations in Section 2. The wave kinetic energy dissipation added to (2.7) is

$$\varepsilon_\phi \overset{\text{def}}{=} -\nu_w \langle |\triangle\phi|^2 \rangle\,. \tag{B 3}$$ {ep_phi}

The kinetic energy dissipation (B 3) is associated only with the incoherent wave field, ϕ', since $\triangle\langle\phi\rangle = 0$. Hyperviscosity also dissipates wave potential energy: the dissipation added to (2.9) is

$$\chi_\phi \overset{\text{def}}{=} -\nu_w \tfrac{\lambda^2}{2} \langle |\boldsymbol{\nabla}\triangle\phi|^2 \rangle\,. \tag{B 4}$$ {chi_phi}

Similarly, the QG kinetic energy dissipation added to (2.10) is

$$\varepsilon_q \overset{\text{def}}{=} -\nu_e \langle q^2 \rangle\,, \tag{B 5}$$ {ep_q}

and the dissipation added to the potential enstrophy equation is

$$\chi_q \overset{\text{def}}{=} -\nu_e \langle (\triangle q)^2 \rangle\,. \tag{B 6}$$ {chi_q}

In all solutions of initial value problems reported in this paper, the dissipative terms (B 3), (B 4), and (B 5) account for less than 1% of the energy tendencies.

B.2. *Numerical methods*

We solve the QG-NIW system (2.1)-(2.3) using a standard collocation Fourier spectral method. In the pseudo-spectral spirit, we evaluate the quadratic non-linearities in physical space, and transform the product into Fourier space. We time march the spectral equations using an exponential time differencing method with a fourth order Runge-Kutta scheme (details in Kassam & Trefethen 2005).

B.3. *Parameters*

REFERENCES

Alford, Matthew H 2001 Internal swell generation: The spatial distribution of energy flux from the wind to mixed layer near-inertial motions. *Journal of Physical Oceanography* **31** (8), 2359–2368.

Alford, Matthew H, MacKinnon, Jennifer A, Simmons, Harper L & Nash, Jonathan D 2016 Near-inertial internal gravity waves in the ocean. *Annual review of marine science* **8**, 95–123.

TABLE 1. Description of parameters of Lamb-Chaplygin simulation.

Parameter	Description	Value
N	Number of modes	512
L_d	Domain size	$2\pi \times 200$ km
$2\pi k_e^{-1}$	Dipole radius	$L/15 \approx 84$ km
U_e	Dipole strength	5×10^{-2} m s^{-1}
U_w	NIW speed	5×10^{-1} m s^{-1}
$(U_e k_e)^{-1}$	Eddy turnover timescale	≈ 3 days
N_0	Buoyancy frequency	5×10^{-3} s^{-1}
f_0	Colioris frequency	10^{-4} s^{-1}
$2\pi \mathrm{m}^{-1}$	NIW vertical wavelength	325 m
ν_e	QGPV biharmonic viscosity	5×10^7 m^4 s^{-1}
ν_w	NIW biharmonic viscosity	5×10^7 m^4 s^{-1}

BARKAN, ROY, WINTERS, KRAIG B & MCWILLIAMS, JAMES C 2016 Stimulated imbalance and the enhancement of eddy kinetic energy dissipation by internal waves. *Journal of Physical Oceanography* (2016).

BÜHLER, OLIVER & MCINTYRE, MICHAEL E 1998 On non-dissipative wave–mean interactions in the atmosphere or oceans. *Journal of Fluid Mechanics* **354**, 301–343.

BÜHLER, OLIVER & MCITYRE, M E 2005 Wave capture and wave–vortex duality. *Journal of Fluid Mechanics* **534**, 67–95.

DANIOUX, ERIC, VANNESTE, JACQUES & BÜHLER, OLIVER 2015 On the concentration of near-inertial waves in anticyclones. *Journal of Fluid Mechanics* **773**, R2.

D'ASARO, ERIC A, ERIKSEN, CHARLES C, LEVINE, MURRAY D, PAULSON, CLAYTON A, NIILER, PETER & VAN MEURS, PIM 1995 Upper-ocean inertial currents forced by a strong storm. part i: Data and comparisons with linear theory. *Journal of physical oceanography* **25** (11), 2909–2936.

FERRARI, RAFFAELE & WUNSCH, CARL 2009 Ocean circulation kinetic energy: Reservoirs, sources, and sinks. *Annual Review of Fluid Mechanics* **41** (1), 253.

FORNBERG, BENGT 1977 A numerical study of 2-D turbulence. *Journal of Computational Physics* **25** (1), 1–31.

KASSAM, ALY-KHAN & TREFETHEN, LLOYD N 2005 Fourth-order time-stepping for stiff pdes. *SIAM Journal on Scientific Computing* **26** (4), 1214–1233.

KLEIN, PATRICE, LLEWELLYN SMITH, STEFAN & LAPEYRE, GUILLAUME 2004 Organization of near-inertial energy by an eddy field. *Quarterly Journal of the Royal Meteorological Society* **130** (598), 1153–1166.

LANDAU, LEV DAVIDOVICH & LIFSHITZ, EVGENII MIKHAILOVICH 2013 *Quantum mechanics: non-relativistic theory*, , vol. 3. Elsevier.

MCWILLIAMS, JAMES C 1984 The emergence of isolated coherent vortices in turbulent flow. *Journal of Fluid Mechanics* **146**, 21–43.

MELESHKO, VV & VAN HEIJST, GJF 1994 On Chaplygin's investigations of two-dimensional vortex structures in an inviscid fluid. *Journal of Fluid Mechanics* **272**, 157–182.

NAGAI, TAKEYOSHI, TANDON, AMIT, KUNZE, ERIC & MAHADEVAN, AMALA 2015 Spontaneous generation of near-inertial waves by the Kuroshio Front. *Journal of Physical Oceanography* **45** (9), 2381–2406.

SHAKESPEARE, CALLUM J & HOGG, ANDREW MCC 2017 Spontaneous surface generation and interior amplification of internal waves in a regional-scale ocean model. *Journal of Physical Oceanography* (2017).

TAYLOR, STEPHANNE & STRAUB, DAVID 2016 Forced Near-Inertial Motion and Dissipation of Low-Frequency Kinetic Energy in a Wind-Driven Channel Flow. *Journal of Physical Oceanography* **46** (1), 79–93.

WAGNER, GL & YOUNG, WR 2016 A three-component model for the coupled evolution of near-

inertial waves, quasi-geostrophic flow and the near-inertial second harmonic. *Journal of Fluid Mechanics* **802**, 806–837.

Xie, J-H & Vanneste, Jacques 2015 A generalised-lagrangian-mean model of the interactions between near-inertial waves and mean flow. *Journal of Fluid Mechanics* **774**, 143–169.

Young, WR & Ben Jelloul, Mahdi 1997 Propagation of near-inertial oscillations through a geostrophic flow. *Journal of marine research* **55** (4), 735–766.